ORIGINAL ARTICLE

Improving the stability of the friction stir channelling technology via a cooled copper backing plate

Catarina Vidal[1,2] · Pedro M. Ferreira[1] · Francisco B. Ferreira[1] · Miguel Buinho[1] · Tiago T. Silva[1] · Telmo G. Santos[1,2]

Abstract

The development of the friction stir channelling (FSC) technology has a potential to revolutionize the manufacturing industry, providing an innovative way to produce continuous sub-surface channels in monolithic components in a single step. However, the process generates heat that can lead to defects and loss of stationarity, affecting the quality of the channels produced and the process' efficiency and control. To address these challenges, a ground-breaking study was conducted using a cooled copper backing plate to adjust the process temperatures and investigate the influence of the temperature on FSC stability. The results of the study showed that the cooled copper backing plate has a significantly higher rate of heat conduction, effectively preventing the processed component from overheating and ensuring that the process maintains its stationarity. When using the steel backing plate, only one combination of process parameters (a rotation speed of 450 rev/min and a traverse speed of 71 mm/min) yielded satisfactory results. Moreover, the use of the cooled copper backing plate allowed for a wider range of process parameters to be employed, resulting in sub-surface channels with higher quality and fewer defects. The 710/71 parameters combination resulted in a lower heat input, while the 900/45 parameters set produced channels with a more rectangular geometry. A rotation speed of 900 rev/min and a traverse speed of 45 mm/min have been shown to be the best choice. This innovative approach to FSC technology represents a major step forward in solid-state manufacturing, envisaging new possibilities for producing longer sub-surface channels with superior quality and greater efficiency.

Highlights

- Conducting the FSC process at low temperature has improved its stability.
- The use of a cooled copper backing plate enabled a broader range of FSC process parameters.
- Longer and stabler leak-free sub-surface channels have been produced in aluminium alloys.

Keywords Friction stir channelling · Low temperature · Cooled backing plate · Sub-surface channels · AA5083-H111

1 Introduction

The friction stir channelling (FSC) has undergone significant development since its initial conception as a manufacturing process for compact heat exchangers [1]. Traditional micro/mini-channel fabrication processes, such as electron beam machining and laser micromachining, are expensive, time-consuming, and often result in an open channel that requires an additional material layer to cover the exposed side. The FSC process offers a low-cost alternative that overcomes these limitations, making it a promising technique for a wide range of applications, including biomedical appliances, electronic cooling systems, and nuclear reactors. To ensure optimal thermohydraulic performance, it is crucial to achieve uniformity in the channel geometry [2–7].

FSC is a manufacturing technology that employs the principles of friction stir welding and processing (FSW/P) [1] to create an internal closed channel, a sub-surface channel, in a single step. This technology allows channels' size and shape control [8]. Mishra [9] was the first to publish a patent in 2005 based on creating a channel through an expansion of the worm-hole defect during FSW. By combining

✉ Catarina Vidal
c.vidal@fct.unl.pt

1 UNIDEMI, Department of Mechanical and Industrial Engineering, NOVA School of Science and Technology, Universidade NOVA de Lisboa, 2829-516 Caparica, Portugal

2 Laboratório Associado de Sistemas Inteligentes, LASI, 4800-058 Guimarães, Portugal

the threaded direction of the pin and the rotation direction of the tool with a shoulder–workpiece clearance, material from the workpiece flows towards the clearance, producing a cavity inside the stirring zone. This cavity is created by the non-consumable tool's rotation due to the clearance between the workpiece and tool shoulder [10].

Since the first patent in 2005 [1], which introduced the first variant of FSC (FSC with shoulder–workpiece clearance), several new variants have been proposed, including FSC without shoulder–workpiece clearance [11], modified friction stir channelling (MFSC) [12, 13], hybrid friction stir channelling (HFSC) [14], and stationary shoulder FSC (SSFSC) [15]. Numerous studies have also been conducted on the process parameters and mechanical properties of channels produced by FSC [7, 10, 16, 17], fatigue testing [18–21], channel formation [13, 22], the forces involved during the process [23–25], and its suitability for the fabrication of heat exchanger devices [26, 27].

Vidal et al. [28] proposed and patented a modified version of the FSC process that achieves greater channel dimensions with increased roughness, leading to improved heat transfer. The authors claimed that by eliminating any clearance between the tool shoulder and the solid component, a certain amount of processed material flows out of the viscoplastic zone, thereby creating the internal channel. The material from the interior of the monolithic component is removed from the treated zone as a self-detachable burr, rather than being deposited on the outer surface of the workpiece. In other words, this method removes material from the workpiece during the FSC process by creating a channel without leaving any clearance [29].

In friction stir-based channelling, a non-consumable tool consisting of a pin and a shoulder is used for material processing. The tool design parameters, such as material, shoulder diameter, pin diameter, shoulder-to-pin diameter ratio, shoulder surface geometry, pin surface geometry, and pin shape, have a significant impact on viscoplastic material flow [30] and heat input conditions [31]. Accurate control of process parameters and material flow is crucial for regulating channel development and optimizing the channels' thermal and mechanical properties. Stability and regularity of channel development over a complex path are critical factors in FSC [25].

In a study developed by Vidal et al. [25], the stability of the FSC process was analyzed using constant position and constant force process control modes on AA5083-H111 plates. It was found that the FSC process was unstable during the forward traverse movement when using position control, with initial plunge loading higher than channelling loading for both modes. Force regulation resulted in minimal changes in the tool's vertical position, and the maximum process temperature was found to be 330 °C. Vishwakarma et al. [19] explored the simultaneous generation of channels during FSW by controlling rotation and traverse speed. The study found that rotational speed played a more significant role in channel generation than traverse speed and that the channels' size and geometry were influenced by the flow pattern around the tool's shoulder and pin, along with machining parameters.

Previous studies conducted by Balasubramanian et al. [10], Vidal et al. [32], Vishwakarma et al. [19], and Rahul et al. [18] have demonstrated that changes in process parameters such as tool traverse speed and rotation speed affect the cross-sectional area and geometry of the channel. Increasing the tool traverse speed initially increases the cross-sectional area, but beyond a certain point, the area starts to decrease. This may be due to insufficient time for the material to flow out of the nugget zone at higher traverse speeds. On the other hand, increasing the rotation speed continuously decreases the cross-sectional area of the channel as the process pitch decreases, hampering the material removal by the tool shoulder scroll and leading to its accumulation between the shoulder's base and the workpiece. This suggests that a higher compacting pressure is applied, improving the shoulder stirring effect and closing the channels. Both traverse and rotation speeds affect the top and the retreating side profiles of the channel, and the traverse speed also affects the channel's tightness. Therefore, changes in process parameters for temperature control may have some drawbacks. Additionally, both, the base material and the backing plate, on which the process is performed, also have a significant influence on the process temperatures and, consequently, on its stability. To the authors' best knowledge, there are no reports of how the backing plate material and temperature influence the FSC process stability.

In this study, three different backing plate materials with different thermal properties were used to assess the influence of this component on the FSC process stability, envisaging its enhancing. Sub-surface channels were produced on AA5083-H111 plates on bakelite, steel, and cooled copper backing plates by FSC. Process temperatures were measured, and channels were characterized to investigate how the process' stability influenced the channels' geometry and properties.

2 Materials and methods

2.1 Materials

Aluminium alloys are commonly used in friction stir-based technologies because of their mechanical properties, which allow them to be processed in the solid-state. In this work, commercial AA5083-H111 plates with dimensions of 203 (rolling direction) × 103 × 10 mm was used as base material.

Table 1 Chemical composition of AA5083-H111 aluminium alloy (wt%) [1, 17, 33, 34]

Elements	Al	Ti	Cr	Zn	Si	Mg	Cu	Fe	Mn
(wt%)	Remnant	0.15	0.05–0.25	0.25	0.4	4-4.9	0.1	0.4	0.4–1

Table 2 Mechanical, electrical and thermal properties of AA5083-H111 aluminium alloy [1, 17, 33]

Properties	AA5083-H111
Density (g/cm^3)	2.65
Melting point (°C)	570
Electrical conductivity (W m^{-1} K^{-1})	121
Modulus of elasticity (GPa)	72
Vickers hardness (HV)	92
Ultimate tensile strength (MPa)	300
Yield strength (MPa)	145
Elongation at break (%)	23
Shear modulus (GPa)	26.9
Shear strength (MPa)	175

2.2 Methods

In this work, the FSC tests were conducted using a modified milling machine with a constant tilt angle of 1°. The experimental setup and implementation of the FSC process were performed according to work conducted by Vidal et al. [17] and can be seen in Fig. 1.

Three different backing plates with different thermal conductivity and diffusivity values were used to study the influence of the process temperature on its stability. The first backing plate was made of bakelite to provide an isolate material and to study the FSC process at higher temperatures. The bakelite backing plate has a thermal conductivity of 0.2 W/m K, and it is depicted in Fig. 1a. The second backing

(a)

Thermal Conductivity: 0.2 W/mK

(b)

Thermal Conductivity: 15.1 W/mK

(c)

Thermal Conductivity: 385 W/mK

Cooling System of the Copper Backing Plate
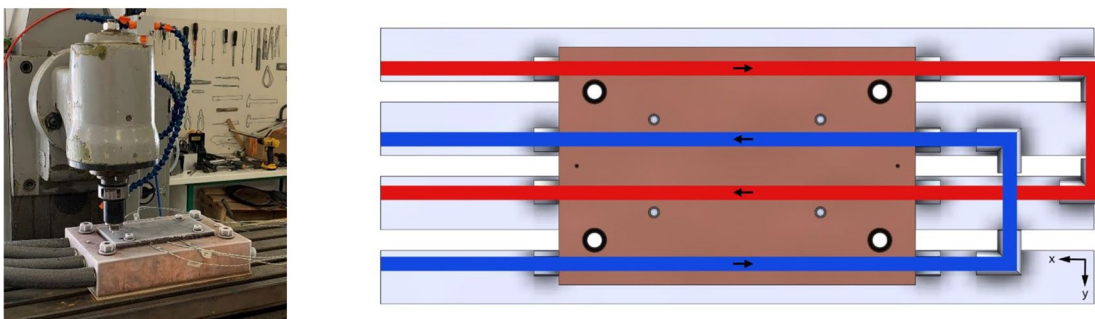
Fig. 1 Different backing plates used to achieve a stationary FSC process: **a** bakelite, **b** steel, and **c** copper backing plates

The nominal chemical composition of the AA5083-H111 is presented in Table 1. The mechanical, electrical, and thermal properties are listed in Table 2. AA5083-H111 was chosen because it is a non-heat treatable, so the mechanical properties after FSC are not degraded, according to the characterization conducted by Vidal et al. [17].

plate was made of CK45 steel, which has a thermal conductivity of 15.1 W/mK. The steel backing plate was used to provide industrial and ambient conditions (Fig. 1b). To ensure that the FSC process is performed at low temperatures, the third backing plate was manufactured of copper, which has a thermal conductivity of 385 W/mK, and a cooling system was installed in the copper backing plate, as depicted in
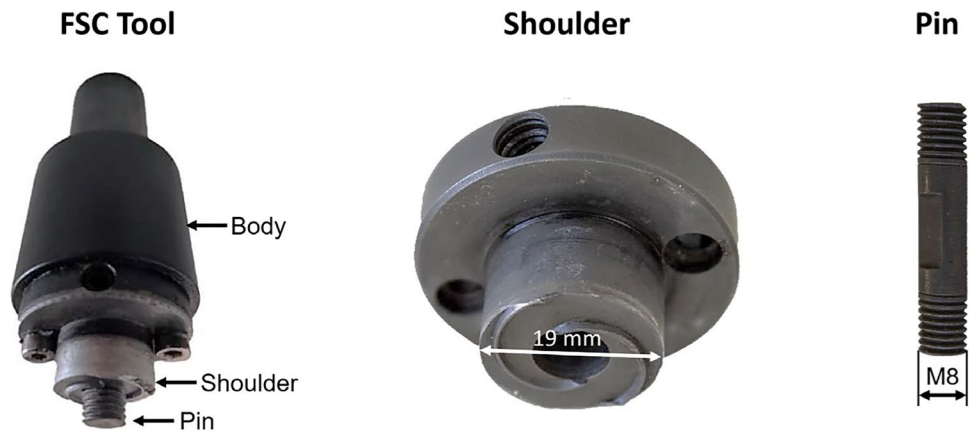
Fig. 2 FSC tool

Fig. 1c. The cooling system (Fig. 1) uses a G13–40 °C coolant that circulates through the holes in the copper backing plate. Therefore, tests were carried out at temperatures ranging from − 8 to − 20 °C, using this cooling system.

A modular non-consumable tool made of H13 steel composed of a left-hand scrolled shoulder with a left-handed cylindrical pin was used for all FSC tests. The tool shoulder had a diameter of 19 mm, and the pin had a M8 thread with a length of 6.7 mm, as it is presented in Fig. 2. The tool rotated in a counter-clockwise direction at the rotation and traverse speeds listed in Table 3, leading to different pseudo heat indexes (PHI). Three sets of experiments were conducted, each with different backing plates. The process parameters for each experiment were determined based on the values presented in Table 3.

In this study, Eq. 1 was used to calculate the PHI for each FSC test. The PHI is a widely used metric for estimating the net heat generated during FSC, based on the ratio of the square of the tool rotation speed to the traverse speed. This approach, which is described in [35], enables us to predict the heating rate during FSC as a function of process parameters. The rotational speed (ω, rev/min) has a significant effect on the heat generated; hence, it is squared in the equation, while the heating rate depends on the traverse speed (v, mm/min) [35]. The PHI values were used to determine the impact of the heat generated during FSC.

$$\text{PHI} = \frac{\omega^2}{v} \ \text{rev}^2/\text{mm. min} \tag{1}$$

2.3 Characterization techniques

2.3.1 Temperature measurements

Temperature measurements were carried out while preforming FSC using four K-type thermocouples placed between the backing plate and the AA5083-H111 plate, two on the advancing side (thermocouples AS) and the others two on the retreating side (thermocouples RS), as depicted in Fig. 3a. To accommodate them, four grooves were machined on the backside of AA5083-H111 plates. Some slots were also added to accommodate and ensure contact between the thermocouple head and the metal plate, allowing for accurate temperature measurement. Figure 3a shows the grooves with the thermocouples. The thermocouple measurements were preformed using a NI-9213 temperature input module, connected to a National Instruments DAQ and assisted by a LabView program for signal data processing.

In addition, a Fluke Ti400 infrared camera was used for surface temperature measurements (Fig. 3b). To ensure appropriate measurements, a layer of mate black paint was applied on the plate surface and an emissivity of 0.95 was set in the camera.
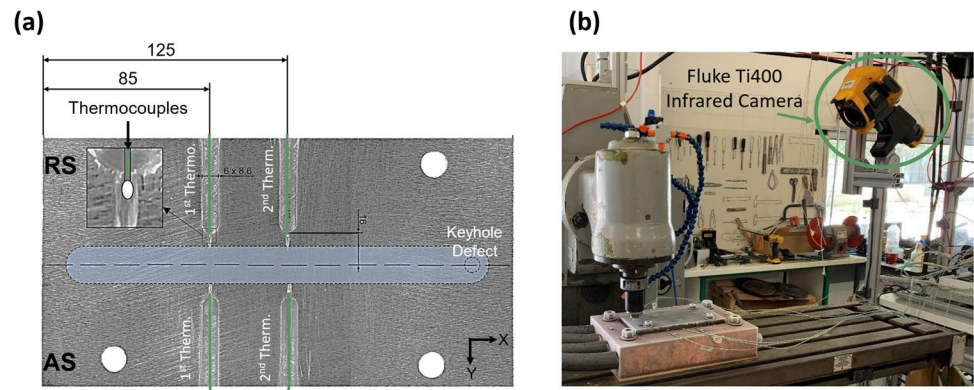
2.3.2 Leakproof testing

Given the possible applications of FSC, such as in the mould industry and heat exchangers, it is essential that the channels

Table 3 The process parameters used to investigate the effect of temperature on FSC stationarity and their corresponding PHI (rev²/mm.min)

Rotational speed, ω (rev/min)	Traverse speed, v (mm/min)				
	45	56	71	90	140
355	-	2250	1775	-	-
450	-	3616	2852	2250	1446
560	6969	5600	4417	-	-
710	-	9002	7100	5601	-
900	18,000	14,464	11,408	9000	-
1120	-	22,400	17,668	13,938	-
1400	-	35,000	27,606	21,778	-
1800	-	57,857	45,634	36,000	-

Fig. 3 Temperature measurement experimental setup: **a** thermocouples and **b** Fluke Ti400 infrared camera setup

produced by this technology are leakproof. The keyhole left by the FSC tool exit was used to introduce compressed air inside the channel at a pressure of 6 bar to perform the leakproof tests. As shown in Fig. 4, the plate was immersed in a water tank, and the channel leakproof was evaluated.

2.3.3 Macro- and microstructural characterization

Following FSC, samples were prepared for several characterization techniques. The macro- and micrography samples were polished according to standard metallographic procedures. Then, macro- and micrography samples were etched in Keller reagent (2 mL HF, 3 mL HCl, 20 mL HNO_3, and 175 mL H_2O). Macro- and micrography optical analyses were performed with a Leica DMI 5000 M inverted optical microscope to examine the unaffected zone (base material), the heat-affected zone (HAZ), the thermo-mechanically affected zone (TMAZ), and the dynamic recrystallization zone.

2.3.4 µCT characterization

The 3D and 2D micro-architectural morphology of the channel was characterized by X-ray microtomography (µCT), using a Phoenix V|TOME|X, GE, according to the procedure conducted by Vidal et al. [36, 37]. The acquired image data were interpreted qualitatively and quantitatively using 3D tomographic reconstruction and analysis software (Volume Graphics 3.04 and SolidWorks software).

2.3.5 Channel internal roughness

The channel internal roughness was measured using a MarSurf M300+RD18 Surface Roughness Tester. However, to access the channel's inner surfaces, a precision cutting disk was used to section the channel, as shown in Fig. 5, allowing access to the top, bottom (Fig. 5b), retreating side (RS) and advancing side (AS) of the channel (Fig. 5a).

2.3.6 Microhardness measurements

Microhardness measurements were performed on a Mitutoyo HM-112 microhardness testing machine according to the ISO 6507-1:2018 standards, to understand how the hardness varies along the various regions of the sample (nugget, TMAZ, and HAZ). The indentations were performed according to the procedure conducted by Vidal et al. [17] and Moreira et al. [38], and the load used was 0.3 kgf applied for 10 s. The spacing between consecutive indentions was 0.5 mm along a line in the middle between the top of the channel and the top surface of the component, as shown in Fig. 6a.

A microhardness map was performed on one of the samples to qualitatively evaluate the variation of the mechanical properties in the main macrostructural regions (nugget, TMAZ, and HAZ). The same parameters were used, but several lines were performed with a vertical spacing of 0.5 mm between them, as shown in Fig. 6b.

2.3.7 Electrical conductivity measurements

The Eddy current technique was used to characterize the electrical conductivity, according to the procedure developed by Sorger et al. [39] and Santos et al. [40]. The electrical conductivity was measured along a straight line along the Y direction. For the Eddy current technique, a pencil probe operating at 2 MHz (corresponding to a penetration depth
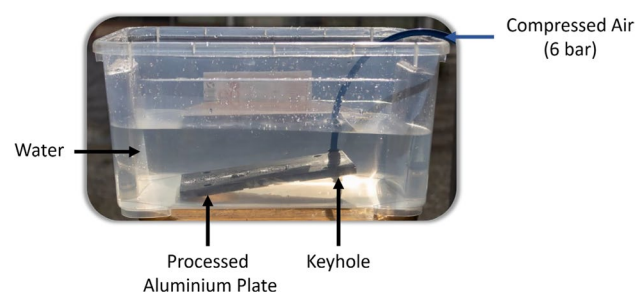

Fig. 4 Leakproof testing apparatus

Fig. 5 Schematic representation of the samples sectioning: **a** section to give access to the retreating and advancing sides of the channel, **b** section to give access to the bottom and top of the channel, and **c** sample before sectioning
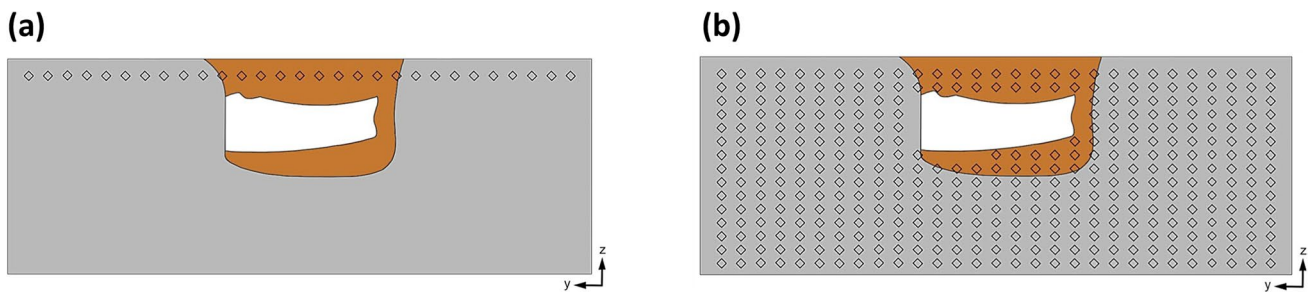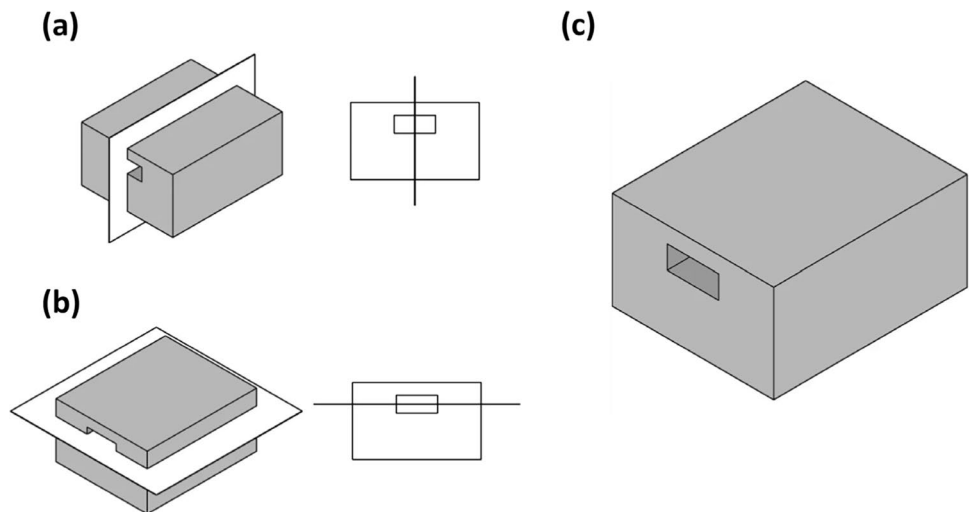

Fig. 6 Schematic representation of a FSC sample indentation: **a** microhardness along a line and **b** microhardness map

of 0.019 mm for this alloy) was used with a NORTEC 600 D impedance analyzer.

3 Results and discussion

3.1 FSC with bakelite and steel backing plates

Firstly, the influence of temperature on FSC stability was carried out using the bakelite and steel backing plates. Based on the results obtained, it can be concluded that during the production of a channel, the conditions of base material do not remain constant, meaning that the temperature of the base material increases as the FSC is carried out. Bakelite is a thermal insulator, which makes it more difficult for the heat generated by the FSC process to dissipate. With the bakelite backing plate, it was not possible to determine a process parameters window that could be considered useful with satisfactory results, so channels could not be obtained.

A series of tests were also conducted using a steel backing plate. With the use of a steel backing plate, the heat generated by the FSC was more easily dissipated. It was possible to establish a narrow window of process parameters that could be considered useful with satisfactory

results for this backing plate, as the conditions for creating non-defective channels can be maintained constant for a longer period when compared to the bakelite backing plate results. The process parameters window obtained with the steel backing plate showed that the process stability was achieved with lower PHI values. Thus, the most satisfactory results were obtained for the following process parameters: 450/71[1], 560/71, 900/71, and 1120/56, with a PHI of 2852, 4417, 11,408, and 22,400 rev^2/mm.min., respectively. The process parameters of 450/71 were considered the best set implemented as its use allowed the manufacture of the longest leak-free channel. It was possible to stabilize the process for parameters with lower PHI values since the heat generated with these parameters was lower and the steel backing plate enabled a better heat dissipation when compared to the bakelite backing plate.

---

[1] To facilitate the identification of the tests throughout the manuscript, it was used a notation that indicates the rotational speed of the tool in rev/min and the traverse speed in mm/min. For example, a test denoted as 450/71 corresponds to a rotation speed of 450 rev/min and a traverse speed of 71 mm/min.

Fig. 7 Temperature recorded using an IR camera Fluke Ti400 of samples obtained with process parameters of 450/71: **a** steel backing plate and **b** bakelite backing plate
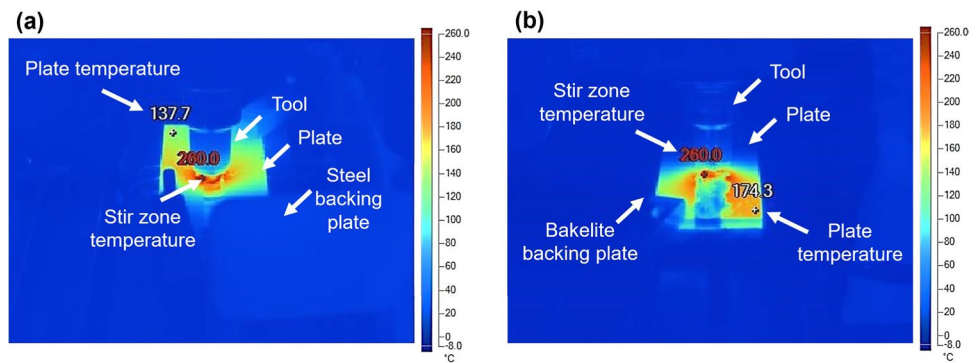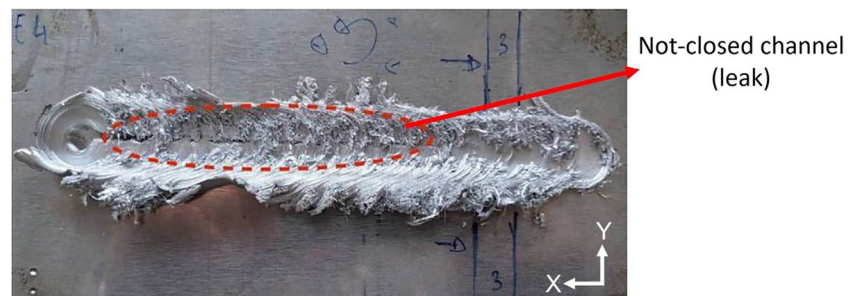

Fig. 8 Not-closed channel

To evaluate the differences between these two backing plates, the temperature field was monitored, as mentioned in Section 2.3.1. From Fig. 7, it can be observed that under the same conditions, the process becomes warmer (174.3 °C compared to 137.7 °C when using the steel backing) when using the bakelite backing plate, being impossible to stabilize the process (the conditions for producing the channel are not constant throughout each processed channel). The process is not stationary. A thermal camera was used to identify a value closer to stir zone. From these results, it can be concluded that the heat extraction capacity using the bakelite backing plate (Fig. 7b) was lower than that obtained when using the steel backing plate (Fig. 7a). For example, in one of the tests carried out, with process parameters of 450/71 using the steel backing plate, the plate's temperature stabilized at around 137.7 °C, as shown in Fig. 7a, and using the bakelite backing plate, the plate's temperature was at around 174.3 °C. It is believed that the temperature in the processed zone is higher as the thermal camera only monitors the surface temperature of the samples.

The leakproof tests determined whether the channel was completely closed and leak-free. This characteristic is relevant as it can enable or disable an industrial application. Before conducting these tests, a visual inspection was carried out because in some circumstances, as in Fig. 8, this test is not necessary to prove that the channel is not airtight. However, even in these situations, this test can be important to understand whether it was possible to achieve some stability in the channel, that is, if it is partially airtight. These channels presented punctual defects, but a stationary state was achieved that allowed to produce some perfectly closed sections. This occurred because it was difficult to keep constant conditions for the channel's formation. For example, the temperature of the backing plate and the aluminum plate increases throughout processing, which makes the material softer. Therefore, it was possible to conclude that the process parameters window changes throughout the channelling stage.

Since the equipment used does not allow for speeds' adjustments during processing, a different strategy was implemented to maintain the conditions constant during channelling, a cooled copper backing plate was developed, and its impact in the FSC is studied in Section 3.2.

Several regions of the channels were analyzed to assess the presence of defects and differences in microstructure. Therefore, it was decided to inspect in greater detail the following zones: the nugget, the advancing side (AS), the retreating side (RS), the base, the corners, and the boundaries between the nugget and the TMAZ.

Figures 9 and 10 correspond to macro- and micrographs of the channels produced with process parameters of 450/71 using steel (Fig. 9) and bakelite (Fig. 10) backing plates. From Figs. 9g and 10g, differences in microstructure were observed in the FSC tool's influence zone when compared to the base material, a change in grain size was identified and will be analyzed below.

In FSC, it is mandatory to obtain a closed channel to consider that the process was carried out in suitable
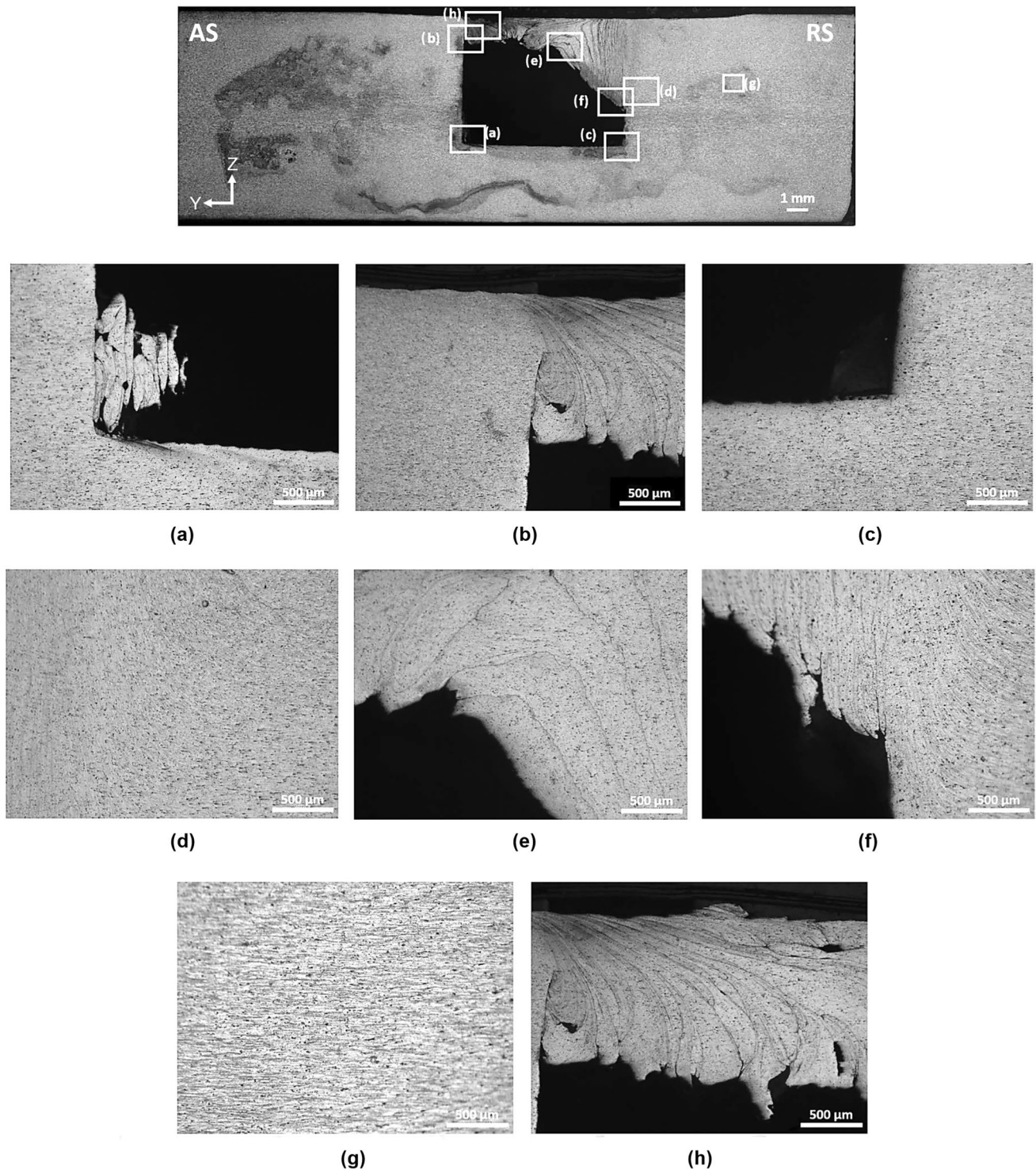
Fig. 9 Optical microscopy images of a samples produced with process parameter of 450/71 using the steel backing plate

conditions. However, defects such as those illustrated in Figs. 9e, f and 10a–c (strongly joined layers) can occur. This can lead to non-leak-proof channels or channels with lower internal strength.

As mentioned in Section 2.1, FSC tests were performed on 10-mm-thick plates with 6.7-mm-long tool pin. Thus, as seen in Figs. 9d, f and 10f, an upward material flow is observed. The explanation for this phenomenon is related to
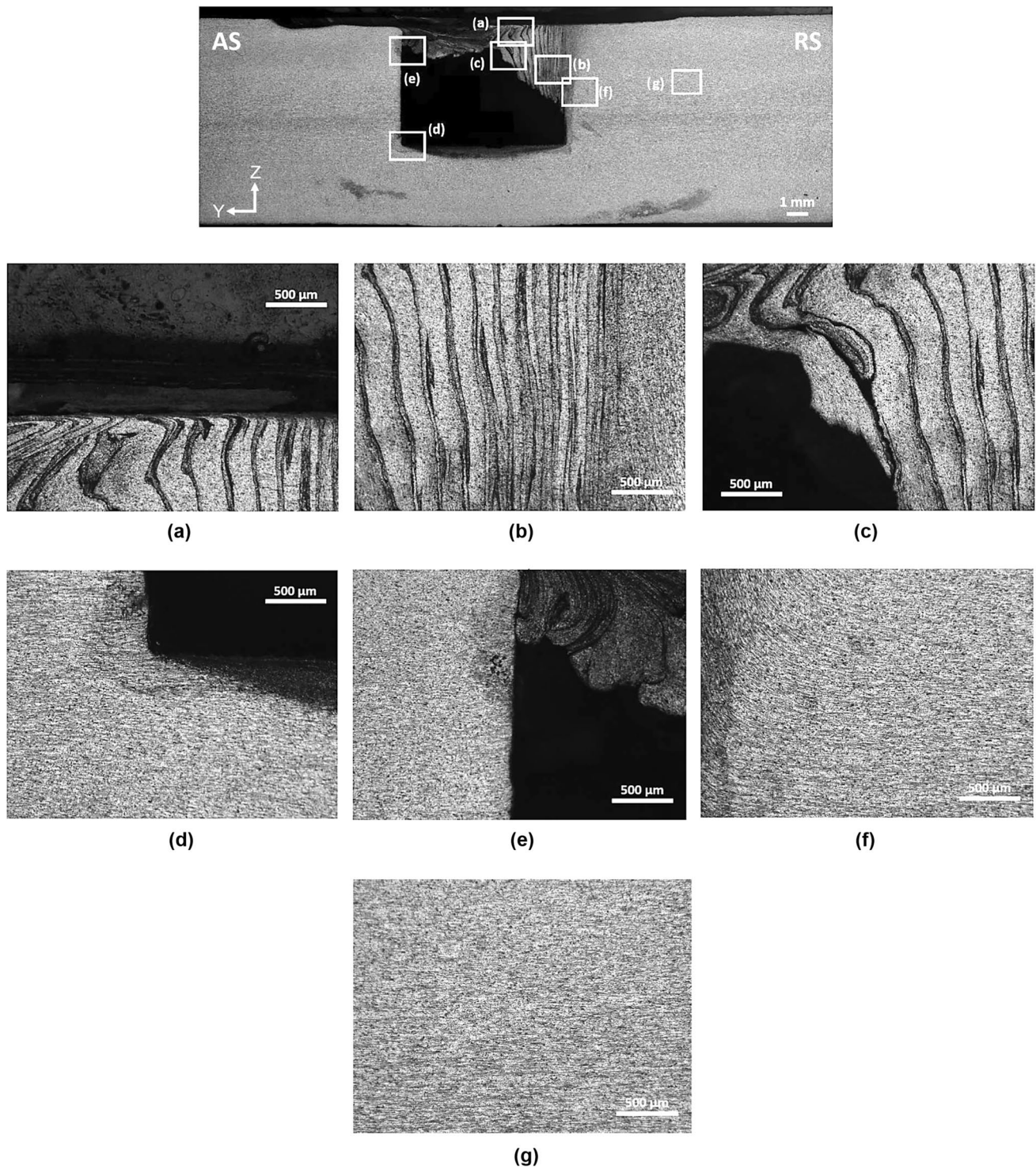
Fig. 10 Optical microscopy images of a samples produced with process parameter of 450/71 using bakelite backing plate

the pin length. When the pin length is longer, the predominant flow will be upward; otherwise, the predominant flow will be downward because the action of the shoulder will prevail over the action of the pin.

During channelling, the nugget zone, as seen in Figs. 9 and 10, undergoes dynamic recrystallization. This results in grain refinement in this zone as well as a variation in hardness (Section 3.2.3).

Table 4 Channel internal roughness measurements carried out on channels obtained with the process parameters of 450/71 using steel and bakelite backing plates

		Ra (μm)	Rmax (μm)
Bakelite backing plate	Advancing side	2.6	27.0
	Channel base	12.1	59.9
Steel backing plate	Advancing side	3.3	25.5
	Channel base	11.5	80.7

Channel internal roughness is a sought-after characteristic in these channels, and it is an important factor for some of their potential industrial applications. Table 4 presents the measurements of internal roughness carried out on channels obtained with the process parameters of 450/71 using bakelite and steel backing plates.

The tests conducted revealed that the advancing side has lower roughness than the channel base. However, both have a significantly lower relative roughness than the top and retreating side of the channel. Macro- and micrographs presented in Figs. 9 and 10 show that the top surface and retreating side of the channels are highly irregular, making it impossible to obtain surface roughness measurements.

The main objective of FSC is to produce sub-surface channels. As previously mentioned, the main applications of these channels are the passage of fluids and the heat transfer from them. Therefore, in addition to roughness being one of the most important parameters, the dimensions of the channels also have great interest. The relevant dimensions of the channels are presented in the Table 5, where the approximation made to the channel geometry can be observed.

The macrographs (Figs. 9 and 10) of the cross-sectional areas of channels with process parameters of 450/71 allowed to compare two tests with only the change from the bakelite to the steel backing plate. With this procedure, the influence of the backing plate on the channel geometry could be verified. From Table 5, a considerable increase in dimension ●e is evident, as will be seen in the following paragraphs, this

factor may be due to position control (pin length). There is no apparent variation caused by the backing plate in these results.

From the measurements carried out, it was possible to investigate the existence of geometric variations along the channel. Therefore, it could be concluded that dimensions ●a and ●b vary along the channels. This fact may be related to position control, which did not remain constant throughout the test (to try to compensate for the increase in temperature). Thus, dimensions ●d and ●e also vary due to the constraint caused by changes in ●a and ●b.

As previously mentioned, a significant factor in the geometric characterization of the channels is the depth/penetration of the pin, which can be calculated by adding the measurements of ●a and ●b.

For each of the backing plates used, hardness measurements were conducted for the channels produced. The results indicated a slight increase in hardness in the HAZ and nugget, with a more noticeable increase in the channels produced using the bakelite backing plate. Specifically, the hardness increased to approximately $\approx$ 95 HV 0.3 in the HAZ and nugget of channels produced with the bakelite backing plate, and to approximately $\approx$ 88 HV 0.3 in those produced with the steel backing plate, as it will be possible to obverse in Section 3.2.3.

3.2 FSC with cooled copper backing plate

With the cooling system, it was found that the process was easier to stabilize compared to tests performed using bakelite and steel backing plates. Throughout the tests, it was observed that the cooled copper backing plate allowed for process stability and, as a result, produced channels in a wider range of parameters combinations. Table 6 shows the combinations of tool rotation speed and traverse speed where the process was stabilized, and a defect-free channel was obtained.

Using the steel backing plate, it was only possible to obtain good results for one parameter combination, 450 rev/

Table 5 Representation of the channel's geometry and their main dimensions

|	Samples	a [mm]	b [mm]	c [mm]	d [mm]	e [mm]	Area [mm²]	Depth [mm]	Typical Channel Geometry
Bakelite Backing Plate*	#1_B	1.5	4.7	7.8	1.9	4.7	32.23	6.2	
	#2_B	1.9	4.0	7.7	1.8	4.1	29.2	5.9	
Steel Backing Plate*	#1_S	1.6	4.7	8.0	2.0	4.9	32.5	6.3	
	#2_S	2.6	4.3	8.1	2.1	5.8	27.6	6.9	
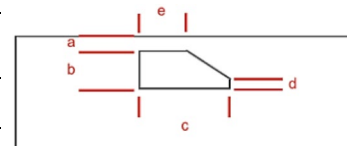
*Two macrographs were obtained to analyze the channel's evolution during its processing

Table 6 Parameter combinations used to investigate the effect of temperature on the stationarity of the FSC process using the cooled copper backing plate

Rotational Speed (ω) [rev/min]	Traverse Speed (v) [mm/min]			
	45	56	71	90
355		✓	✓	
450		✓	✓	
560	✓	✓	✓	
710		✓	✓	✗
900	✓	✓	✓	✓
1120		✓	✓	✓
1400		✓	✓	✗
1800		✗	✗	

The parameters combinations that resulted (✓) and did not result (✗) are also identified

Fig. 11 Temperature recorded using experimental setup with the thermocouples on the advancing and retreating sides: **a** cooled copper backing plate and process parameters of 450/56 and **b** steel backing plate and process parameters of 450/71
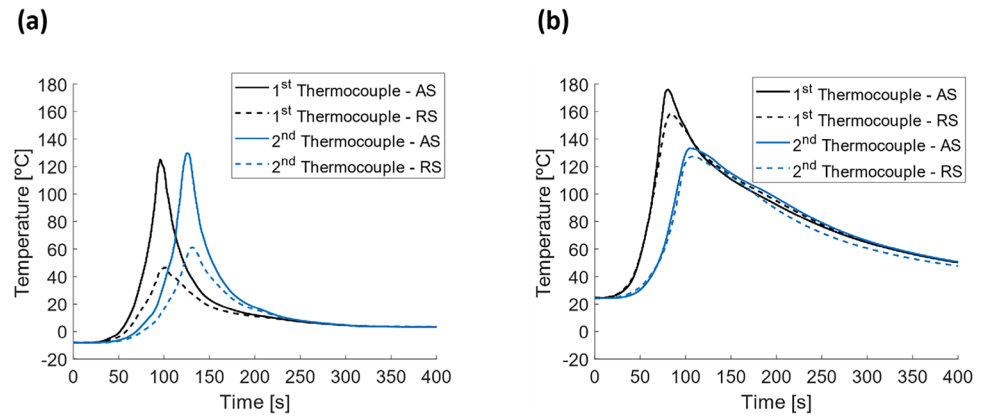
min of rotation speed and 71 mm/min of traverse speed. However, using the same material, equipment, and tool but changing the steel backing plate to a cooled copper backing plate, it became possible to obtain good results with various set of process parameters.

For a traverse speed of 90 mm/min, and because this can be considered a high traverse speed for this technology, there was an increased difficulty in stabilizing the process, and channels could not be produced without defects at 1400/90 and 710/90 conditions.

Increasing the rotation speed for constant traverse speeds (increasing the heat input of the process) made the process easier to stabilize and produced channels with better quality. However, for very high heat inputs (1800/56 and 1800/71 tests), it was not possible neither stabilize the process nor produce non-defective channels.

Figure 11a shows the temperature evolution over time measured by thermocouples during the 450/56 test using the copper backing plate. The temperature differences between the retreating (1st thermocouple–RS and 2nd thermocouple–RS) and advancing sides (1st thermocouple–AS

and 2nd thermocouple–AS) occur because, in this test, the distance between the tool and the AS thermocouples was greater than the distance to the RS thermocouples.

Due to the high thermal diffusivity of copper and the circulation of the cooling fluid, the time it takes for heat to flow out of the processing zone is greatly reduced. At the 2nd thermocouple–AS from the point with the highest temperature, a temperature decreases of 80.93 °C was recorded in 30 seconds, resulting in a cooling rate of 2.70 °C/s.

In the test with the steel backing plate, Fig. 11b, it can be observed that due to the lower heat extraction capacity of this backing plate, the cooling rate is lower. At 1st thermocouple–AS, from the point with the highest temperature, a temperature decreases of 41.06 °C was recorded in 30 s, resulting in a cooling rate of 1.37 °C/s. This causes the temperatures to remain high for a longer period, which causes the component to heat up more and the process lose its stationarity.

Two examples were used with different traverse speed; however, the test with the cooled copper backing plate had a lower traverse speed, which makes the process slower

Fig. 12 Experimental thermogram obtained by IR camera Fluke Ti400 using **a** temperature recorded using the copper backing plate and process parameters of 450/56 and **b** temperature recorded using the steel backing plate and process parameters of 450/71
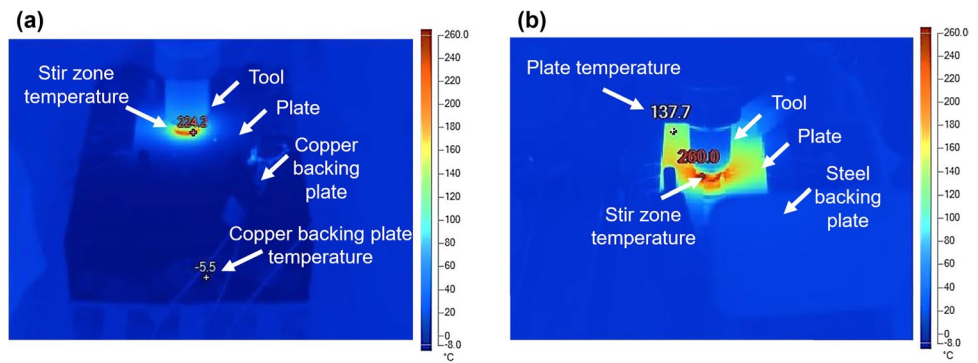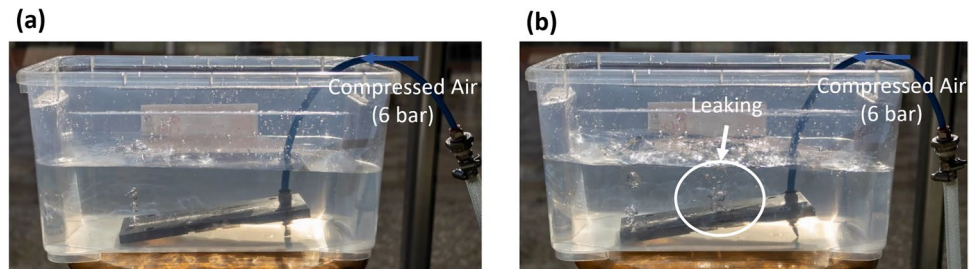

Fig. 13 Leakproof testing: **a** cooled copper backing plate and process parameters of 450/56 and **b** steel backing plate and process parameters of 450/71

with higher heat input, accentuating the differences in heat flow between the two examples.

From the experimental thermogram presented in Fig. 12, it was possible to analyze the surface temperatures during the process. The warmest point at each time was recorded by the IR camera Fluke Ti400 in tests with the same process parameters but with different backing plates. It was observed that the highest temperatures measured during the process are lower when using the cooled copper backing plate. The highest temperature reached with the cooled copper backing was 224.2 °C, which is lower compared to that measured with the steel backing plate, which was 260 °C.

In the experimental thermogram of test 450/56, shown in Fig. 12a, it is possible to observe that the copper backing plate, when cooled, generates a high thermal gradient. This means that high temperatures (represented in shades of green and red) are always near the tool (where heat is generated) and rapidly decrease, due to the high heat extraction capacity of the cooling system at the backing plate and the thermal diffusivity of copper. This is not visible when using the steel backing plate, as shown in Fig. 12a, where a lower thermal gradient is observed when compared to the test with the cooled copper backing plate. With the steel backing plate, high temperatures (represented in shades of green and red) are observed from the tool to the end of the component being processed.

By using the cooled copper backing plate, the process remained stationary as the tool progressed. As a result, by excluding the initial and final zones, which are usually more

prone to defects, and only considering the stable zone of the process, it was possible to obtain leak-free channels.

Figure 13 shows examples of the results of the leakproof tests, where Fig. 13a shows a leak-free channel, and Fig. 13b shows a channel with several defects along its length, which did not pass the leakproof test.
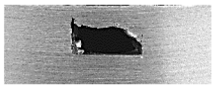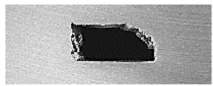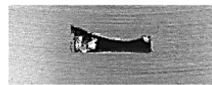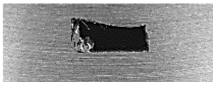
3.2.1 Geometry characterization

From Table 7, it can be observed that as the tool's rotational speed increases, the channel geometry changes from trapezoidal to rectangular. Comparing the results presented in Tables 7 and 3, it is clear that channels with a more rectangular geometry were produced with higher PHI, which indicates higher heat input. Therefore, it can be concluded that the FSC with a cooled copper backing plate benefits from an increase in heat input. However, as mentioned earlier, the process cannot be stabilized and channels without defects cannot be produced at very high heat inputs.

After tests were performed, samples were sectioned, and the geometries of the channels were inspected. From the process parameters window (Table 7) obtained using the copper backing plate, it was possible to perceive that the 900/45 sample presented a channel with the most rectangular geometry.

The variation of the channel area with traverse speed and rotational speed can be observed in Figs. 14 and 15. Changing these parameters affects the channel's cross-sectional area, as noted by several authors [10, 17–19]. It was concluded that increasing the traverse speed increases the cross-sectional area up to a certain point, after which

Table 7 Channels produced by FSC with the cooled copper backing plate

Rotational Speed (ω) [rev/min]	Traverse Speed (v) [mm/min]							
	45		56		71		90	
	(AS)	(RS)	(AS)	(RS)	(AS)	(RS)	(AS)	(RS)
355								
450								
560								
710								
900								
1120								
1400								

Fig. 14 Variation of channel area with traverse speed for different tool rotational speeds
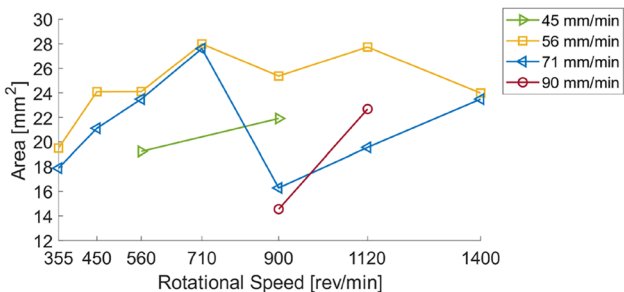
Fig. 15 Variation of channel area with rotational speed for different tool traverse speeds

the cross-sectional area starts to decrease. Vishwakarma et al. [19] suggested that this may be due to insufficient time for the material to exit the nugget zone due to high traverse speeds. This trend is also observable in the results obtained with the use of the cooled copper backing plate, especially for the channels obtained with rotational speed of 900 and 1120 rev/mm, as highlighted in Fig. 14.

On the other hand, increasing the rotational speed of the tool continuously decreases the cross-sectional area of the channel, according to some authors [10, 17–19]. The results presented in Fig. 15 with the use of the cooled copper backing plate showed a similar trend. For the channels obtained with traverse speeds of 45, 56, and 90 mm/min, this trend is evident. However, in the case of channels obtained with a traverse speed of 56 mm/min, the area of the channels tends to stabilize for rotational speeds above 710 rev/mm. For the channels obtained with a traverse speed of 71 mm/min, the same trend is evident for rotational speed below 71 mm/min, but there is a significant reduction in the area for rotational speed above 710 rev/mm, probably related to the sensitivity of the FSC to small variations in the vertical force [25] applied during the production of the channels.

Therefore, the highest channel area that could be produced was achieved using the following process parameters:
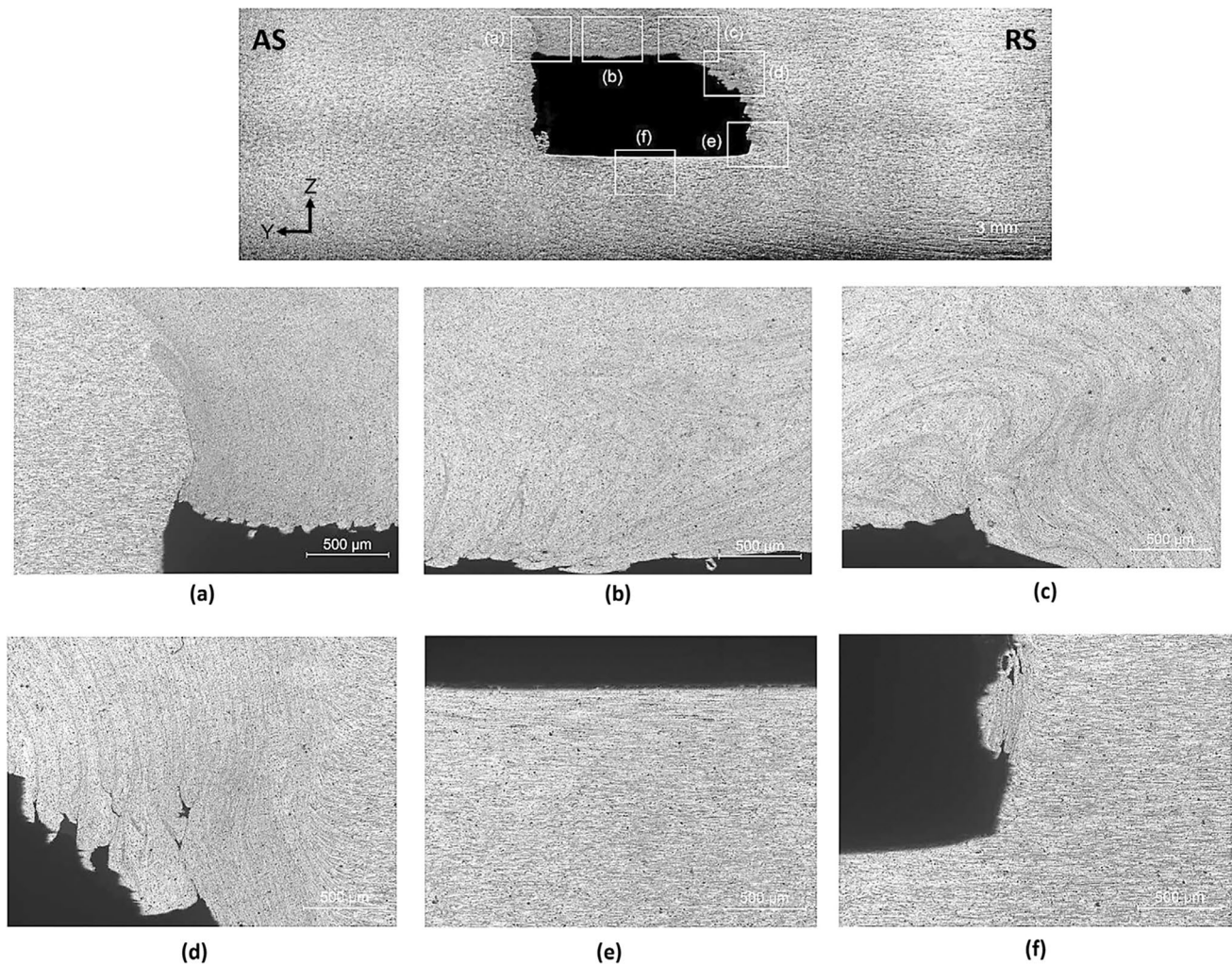
Fig. 16 Optical microscopy images of a samples produced with process parameter of 710/71 using the cooled copper backing plate

710/71 and 710/56. The channel obtained with process parameters 710/71 has a lower heat input (PHI), as can be observed in Table 3. However, the process parameters of 900/45 allow for the production of channels with a more rectangular geometry, which will be later analyzed herein.

3.2.2 Metallographic characterization

Macro- and micrographs of channels produced with the cooled copper backing plate and process parameters of 710/71 and 900/45 are shown in Figs. 16 and 17, respectively. Thus, to understand the presence of defects and differences in microstructure, several zones of these channels were detailed analyzed, including the nugget, advancing and retreating sides, base, corners, and boundaries between the nugget and the TMAZ.

At the interface between the nugget and the TMAZ (observed in Figs. 16a, d and 17a, b, d,), dynamic

recrystallization occurs due to the high temperatures and severe plastic deformations experienced by this region during the process, i.e., the nucleation and growth of new grains. In contrast, the TMAZ experiences temperatures and plastic deformations that are not sufficient for recrystallization.

The deformation in the advancing side is more intense than in the retreating side, as evidenced by the greater contrast at the interface between the nugget and the TMAZ in the advancing side (Figs. 16a and 17a, b) compared to the retreating side (Figs. 16d and 17d).

Compared to the results obtained with steel backing plate (Fig. 9), channels produced with the cooled copper backing plate exhibit a better-defined upper wall and significantly reduced cracking at the top channel of the advancing side (Fig. 9b).

3.2.3 Microhardness measurements

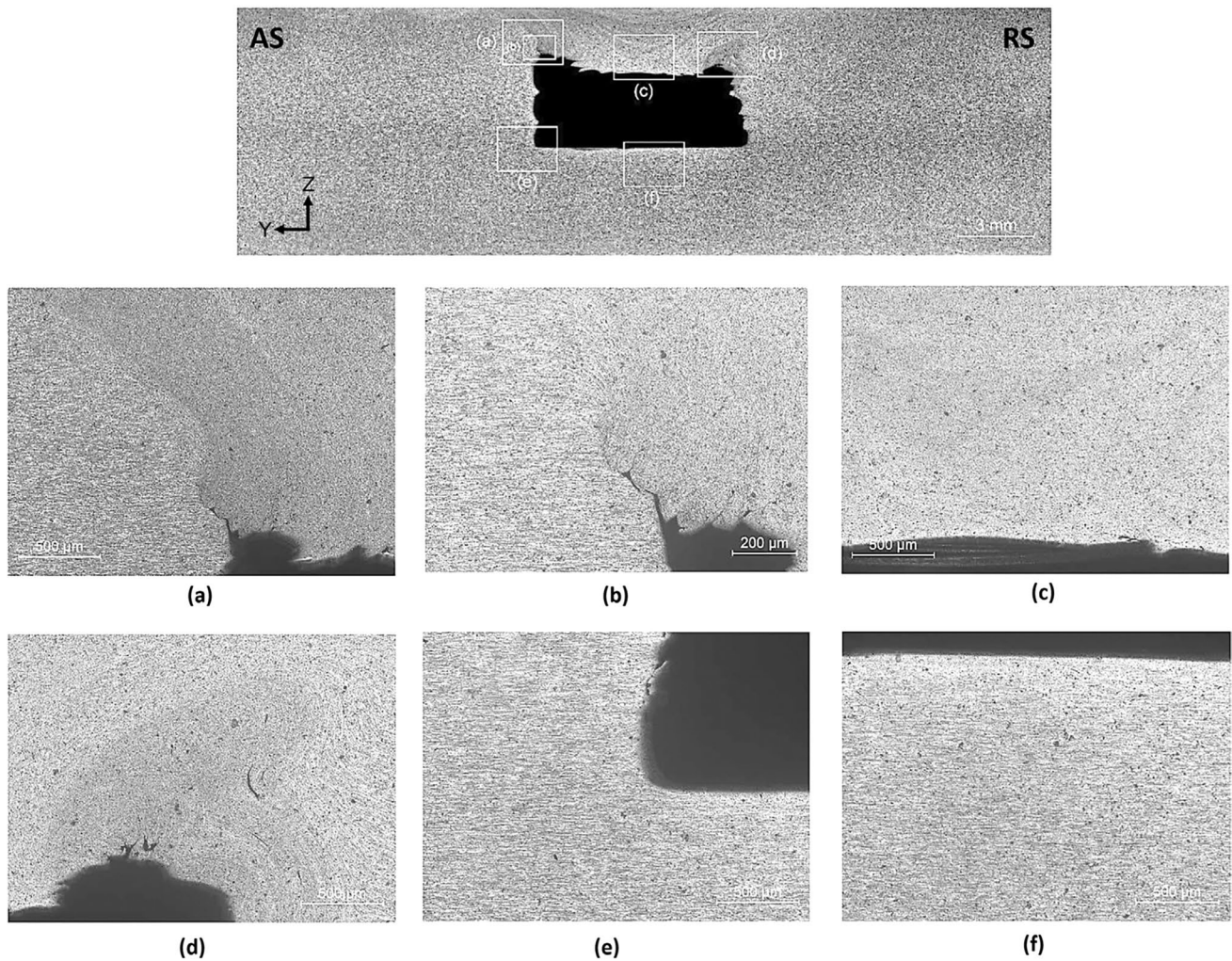Figure 18 shows the microhardness profiles obtained in samples produced with the process parameters of 450/71 using

Fig. 17 Optical microscopy images of a samples produced with process parameter of 900/45 using the cooled copper backing plate

Fig. 18 Microhardness profile along the *Y* direction of the plates obtained with parameter process of 900/45, 710/71, 1120/90, and 1400/56 using the cooled copper backing plate
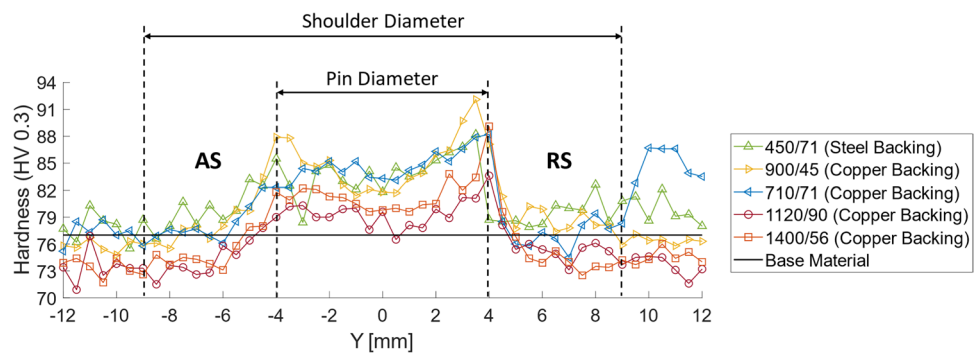
the steel backing plate, in four test samples produced with the cooled copper backing plate, and the average value of the microhardness obtained for the base material.

The use of a backing plate that allows for higher heat extraction, particularly the cooled copper backing plate, does not have a significant impact on the microhardness profile. With both the copper and the steel backing plates, there is an increase in hardness in the nugget zone due to the refinement of the grain caused by dynamic recrystallization, while the remaining material has a hardness similar to that of the base material. This hardness profile, although uncommon in aluminium alloys, was also verified by Torzewski et al. [41], where an FSW sample of the same aluminum alloy used in this work was used.
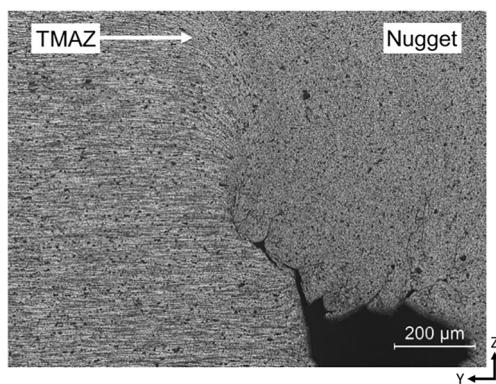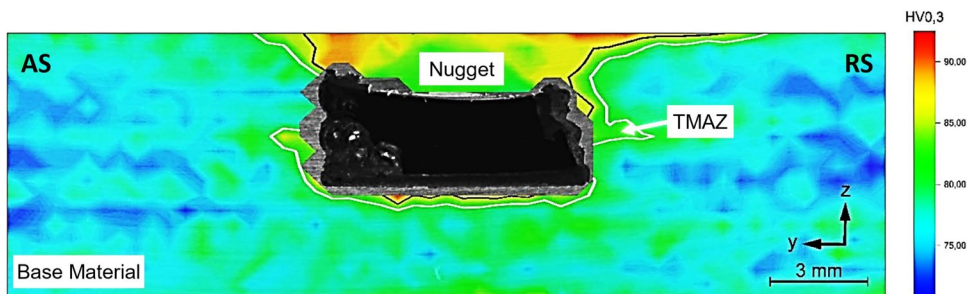
Fig. 19 Optical microscopy image of a channel's advancing side produced with process parameter of 900/45 using the cooled copper backing plate

In the transition between the base material to the nugget zone, an inclined zone can be observed where there is a gradual increase in microhardness, as shown in Fig. 18, which corresponds to the TMAZ. Figure 19 shows the described transition zone corresponding to the TMAZ.

In the obtained microhardness profiles, neither the steel backing plate nor the cooled copper backing plate tests showed the presence of the HAZ, where a loss of hardness is typically observed compared to the base material.

Based on the results presented in Fig. 18, the sample with the highest microhardness was the one processed with the parameters of 900/45. Therefore, a more detailed mapping of this sample was carried out, as shown in Fig. 20.

Figure 20 shows the microhardness map obtained from a sample produced with process parameters of 900/45. This map provides a clearer view of the nugget region (outlined in black) and the TMAZ region (outlined in white). It is not possible to draw conclusions regarding the HAZ region, as there is no significant decrease in hardness compared to the base material.

3.2.4 Channel internal roughness measurements

Tables 8, 9, 10, and 11 show the internal roughness measurements of four channels. Due to the high roughness exhibited by both the advancing and retreating sides wall, and the top wall, it was not possible to obtain reliable results using the MarSurf M300 + RD18 Surface Roughness Tester. However, for the bottom of the channel, its roughness was measurable, and the channel produced with process parameters of 710/71 showed the lowest roughness. It should be noted that the average roughness (Ra) is the arithmetic average of the individual heights and depths of the profile from the mean line. Rz is the difference between the highest peak and

Fig. 20 Microhardness map of channel produced with process parameters of 900/45 using copper backing plate

Table 8 Internal roughness measurements of channel produced with process parameters of 710/71

Channel with process parameters of 710/71				
Channel	**Advancing Side**	**Bottom Wall**	**Retreating Side**	**Top**
Ra (μm)	-	1.724 ± 0.400	-	-
Rq (μm)	-	2.295 ± 0.507	-	-
Rz (μm)	-	10.28 ± 2.906	-	-

Table 9 Internal roughness measurements of channel produced with process parameters of 900/45
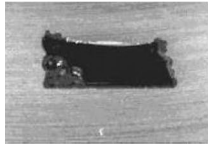
Channel with process parameters of 900/45				
Channel	**Advancing Side**	**Bottom Wall**	**Retreating Side**	**Top**
Ra (μm)	-	3.884 ± 0.638	-	-
Rq (μm)	-	6.335 ± 0.898	-	-
Rz (μm)	-	28.00 ± 6.642	-	-

Table 10 Internal roughness measurements of channel produced with process parameters of 1120/90
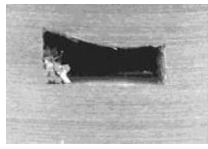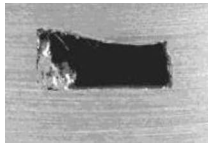
Channel with process parameters of 1120/90				
Channel	**Advancing Side**	**Bottom Wall**	**Retreating Side**	**Top**
Ra (μm)	-	3.233 ± 0.232	-	-
Rq (μm)	-	3.938 ± 0.258	-	-
Rz (μm)	-	17.130 ± 1.901	-	-

Table 11 Internal roughness measurements of channel produced with process parameters of 1400/56

Channel with process parameters of 1400/56				
Channel	**Advancing Side**	**Bottom Wall**	**Retreating Side**	**Top**
Ra (μm)	-	4.531 ± 1.217	-	-
Rq (μm)	-	5.962 ± 1.585	-	-
Rz (μm)	-	26.730 ± 4.329	-	-

the lowest valley in the surface. Root mean square roughness (Rq) is the square root of the sum of the squares of the individual heights and depths from the mean line.

Following an initial analysis, it is observed from the channel interior images that an increase in the tool rotation speed results in a better finishing on the top wall of the channel. Figure 21 illustrates the correlation between the tool rotation speed and the finish of the channel top. It can also be observed that the PHI does not influence the finish of the channel top.

Furthermore, it is also observed that in all four samples analyzed (710/71, 900/45, 1120/90, and 1400/56) there are processed material that was not removed during the process, in the corner where the top wall meets the advancing
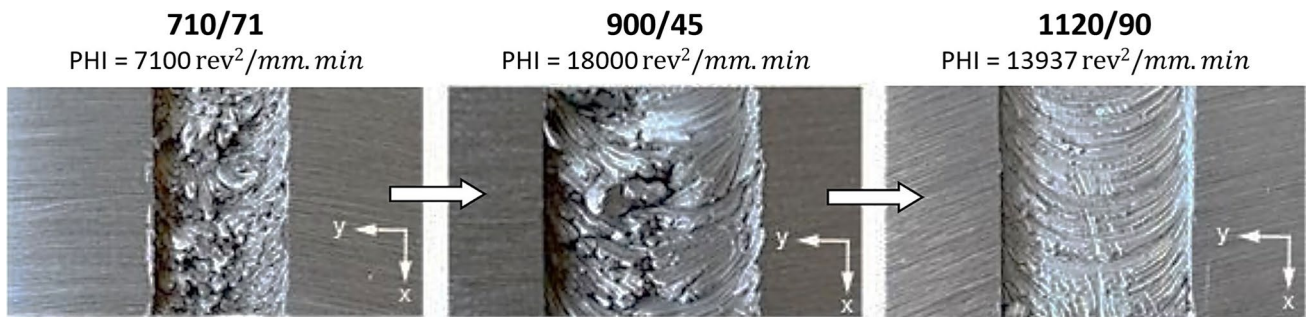
710/71
PHI = 7100 rev²/mm. min

900/45
PHI = 18000 rev²/mm. min

1120/90
PHI = 13937 rev²/mm. min

Fig. 21 Comparison of the top of several channels

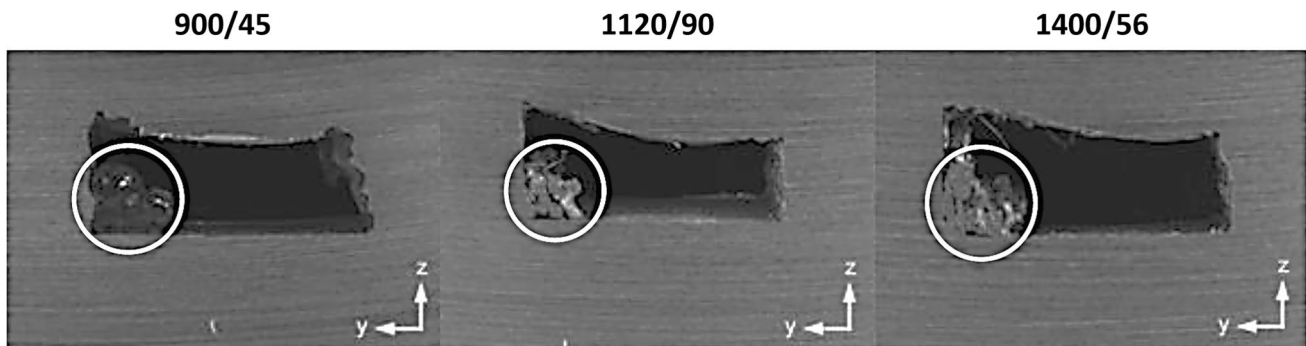**900/45**

1120/90

1400/56

Fig. 22 Example of samples with processed material not removed during the FSC

side wall, and this same material can be seen in all channels in the same region, as shown in Fig. 22. It should be noted that the fluid flowing through channels with this unremoved processed material may become contaminated. Figure 22 shows in detail, highlighted in white, the mentioned unremoved processed material in three samples.

After conducting a second analysis and comparing the roughness values obtained for the bottom wall of the channel using a steel backing plate (Table 4), it was found that the values obtained using the cooled copper backing plate were lower. This may be due to the stability provided by the cooled copper backing plate, which keeps the process stationary, or because the material processed adheres less to the channel due to the lower temperatures that occur in the process when using the cooled copper backing plate. However, it is important to note that there may be other reasons for the decrease in roughness that require further investigation.

One of the significant applications of FSC is the manufacturing of components with heating/cooling channels. Therefore, producing channels with lower roughness values, although potentially reducing fluid pressure losses, is not necessarily beneficial as it may result in a lower heat transfer.

3.2.5 μCT characterization

The channel produced with process parameters of 900/45 can be visualized in the μCT volume model image shown in Fig. 23. The channel can be imagined as consisting of four different sides: the advancing-side wall, the retreating-side wall, the top, and the bottom. For a better view, the advancing side wall (Fig. 24a), retreating side wall (Fig. 24b), bottom wall (Fig. 24c), and top wall (Fig. 24d) of the channel are sectioned off from the μCT volume model image, as shown in Fig. 24.

The channel has a constant width and height throughout its length, with an average width of 4 mm and an average height of 7.5 mm. Although there is a small variation in the height of the wall, as seen in Fig. 24a, b, this is a result of a slight variation in the position of the tool and does not affect the stability of the FSC. It can be concluded that implementing a position control would address such variations.

The results of μCT show that processing with the refrigerated copper backing produced channels with a constant and rectangular geometry. Flow patterns are visible on the advancing side (Fig. 24a) and retreating side walls (Fig. 24b), which are characteristic of the FSC.

Fig. 23 μCT volume model images of a sample processed with process parameters of 900/45: advancing side (AS) wall, retreating side (RS) wall, top wall, and bottom wall
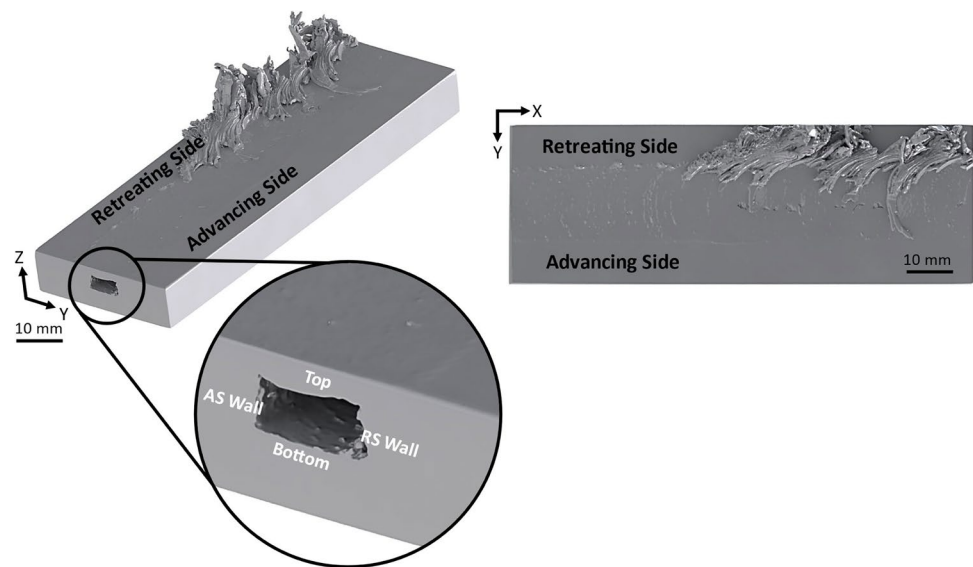
Regarding the surface quality of the channel shown in Fig. 24 and in addition to the results obtained in the channel internal roughness measurements (Section 3.2.4), it was only possible to notice flow patterns that are characteristic of the FSC process, as well as some small residues that were not removed during the processing.

4 Conclusions

Although, the FSC technology is still in development and several studies have been conducted on various aspects, this study is the first one investigating the importance of the backing plate in this technology and its stationarity. The findings have significant implications for the forthcoming development and future applications of this technology in the industry.

It was found that it is impossible to determine a useful process parameters window for the bakelite backing plate because the conditions for creating non-defective channels are not achieved. The process parameters window varies over time due to the increasing temperature of the process, which is compounded by the higher thermal resistance inherent in bakelite.

Using the steel backing plate, only one combination of process parameters (450 rev/min rotation speed and 71 mm/min traverse speed) yielded satisfactory results. However, by replacing the steel backing plate with a cooled copper backing plate while keeping the same material, equipment, and tool, it became possible to achieve good results with multiple sets of process parameters.

However, using a cooled copper backing plate allowed to produce channels with the FSC technology over a much wider range of parameters compared to when the process was carried out on a steel backing plate. The temperature at the stir zone (near the tool) remained high with a cooled copper backing plate since a certain temperature is necessary to achieve the viscoplastic regime. However, the significant difference was found in the proximity of stir zone. A cooled copper backing plate led to a higher heat conduction rate, preventing the component from overheating and maintaining stationarity throughout channelling stage.

The use of a cooled copper backing plate did not significantly change the microhardness profile compared to the steel backing plate. The reduction in internal roughness on the channels' bottom could lead to a reduction in pressure drop when applying FSC to produce channels in components for cooling/heating purposes. However, this reduction may also reduce heat transfer, which is not necessarily beneficial. The highest channel area was achieved with the process parameters 710/71 and 710/56. The 710/71 parameters resulted in a lower heat input (PHI), while the 900/45 parameters produced channels with a more rectangular geometry. So, the 900/45 parameters have been shown to be the best choice.

The authors declare that the present study is original, without any kind of plagiarism and/or inappropriate data manipulation/falsification form and has not been divided in several parts. The authors also declare that the work reported in this paper has not been published previously, and is not under consideration for publication elsewhere, in English or in any other language.

Fig. 24 3D representation obtained by μ-CT of internal walls of a channel processed with process parameters of 900/45
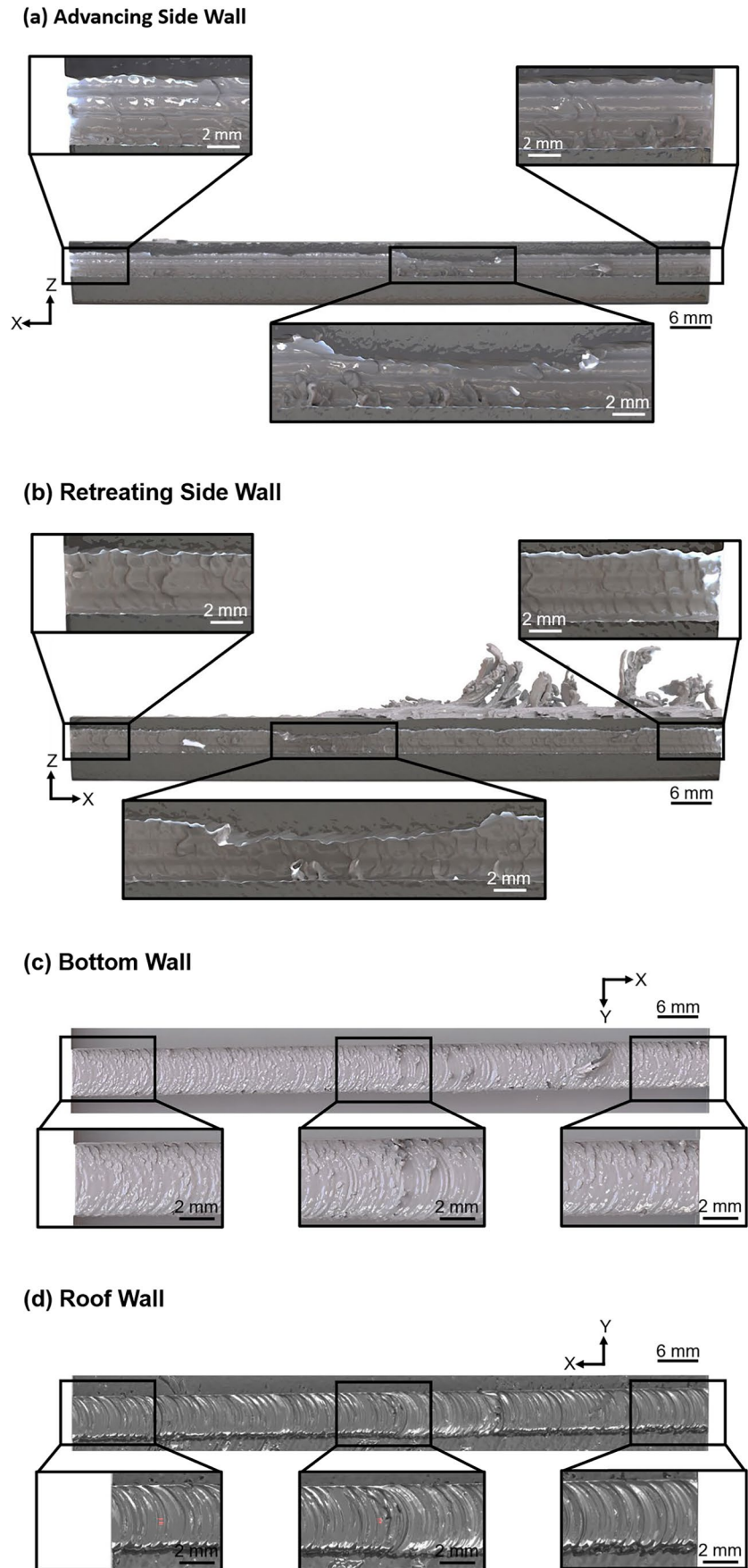
(a) Advancing Side Wall

(b) Retreating Side Wall

(c) Bottom Wall

(d) Roof Wall

Declarations

Consent to participate This is not applicable.

Consent for publication The authors declare that they consent the publication of the work reported in this paper.

Competing interests The authors declare no competing interests.

References

1. Vilaca P, Gandra J, Vidal C (2012) Linear friction based processing technologies for aluminum alloys: surfacing, stir welding and stir channeling. Alum Alloy New Trends Fabr Appl InTech. https://doi.org/10.5772/52026

2. Dixit T, Ghosh I (2015) Review of micro- and mini-channel heat sinks and heat exchangers for single phase fluids. Renew Sust Energ Rev 41:1298–1311. https://doi.org/10.1016/j.rser.2014.09.024

3. Pandya S, Gurav S, Hedau G, Saha SK, Arora A (2020) Effect of axial conduction in integral rough friction stir channels: experimental thermo-hydraulic characteristics analyses. Heat Mass Transf 56:1725–1738. https://doi.org/10.1007/s00231-019-02788-7

4. Rashidi A, Mostafapour A (2015) Influence of tool pin geometry and moving paths of tool on channel formation mechanism in modified friction stir channeling technique. Int J Adv Manuf Technol 80:1087–1096. https://doi.org/10.1007/s00170-015-7049-7

5. Salimi S, Haghpanahi M, Bahemmat P (2018) Fabrication of cooling channels employing worm voids caused by friction stir based process: considering cooling and fluid parameters. J Manuf Process 35:61–70. https://doi.org/10.1016/j.jmapro.2018.07.016

6. Mei F, Parida PR, Jiang J, Meng WJ, Ekkad SV (2008) Fabrication, assembly, and testing of Cu- and Al-based microchannel heat exchangers. J Microelectromech Syst 17:869–881. https://doi.org/10.1109/JMEMS.2008.924276

7. Vidal C, Infante V, Vilaça P (2012) Metallographic characterization of friction stir channels. Mater Sci Forum 730–732:817–822. https://doi.org/10.4028/www.scientific.net/MSF.730-732.817

8. Mehta KP, Vilaça P (2022) A review on friction stir-based channeling. Crit Rev Solid State Mater Sci 47:1–45. https://doi.org/10.1080/10408436.2021.1886042

9. Mishra RS. Integral channels in metal components and fabrication thereof. US6923362B2, 2005.

10. Balasubramanian N, Mishra RS, Krishnamurthy K (2009) Friction stir channeling: characterization of the channels. J Mater Process Technol 209:3696–3704. https://doi.org/10.1016/j.jmatprotec.2008.08.036

11. Vidal C, PV. (2011) Processo de abertura de canais internos contínuos em componentes maciços sem alteração da cota de superfície processada e respectiva ferramenta modular ajustável. Patent 105628:15

12. Rashidi A, Mostafapour A, Salahi S, Rezazadeh V (2013) Modified friction stir channeling: a novel technique for fabrication of friction stir channel. Appl Mech Mater 302:365–370. https://doi.org/10.4028/www.scientific.net/AMM.302.365

13. Rashidi A, Mostafapour A, Rezazadeh V, Salahi S (2013) Channel formation in modified friction stir channeling. Appl Mech Mater 302:371–376. https://doi.org/10.4028/www.scientific.net/AMM.302.371

14. Heikki KARVINEN PV. Non-consumable tool and a process for solid-state production of a channel and a weld joint, and a structure of at least two components based on originally bulk components of similar, or dissimilar, materials. US11052480B2, 2017.

15. Gandra J. Method and apparatus for creating channels in workpieces. US11020817B2, 2016.

16. Vidal C, Infante V, Vilaça P (2011) Mechanical characterization of friction stir channels under internal pressure and in-plane bending. Key Eng Mater 488–489:105–108. https://doi.org/10.4028/www.scientific.net/KEM.488-489.105

17. Vidal C, Infante V, Vilaça P (2019) Metallographic and morphological characterization of sub-surface friction stirred channels produced on AA5083-H111. Int J Adv Manuf Technol 105:2215–2235. https://doi.org/10.1007/s00170-019-04459-7

18. Rahul M, Saikiran M, Ashok KP (2021) Scrutinize on friction stir channeling performance in dissimilar aluminum amalgams. Mater Today Proc 39:91–94. https://doi.org/10.1016/j.matpr.2020.06.311

19. Vishwakarma P, Upadhyay V, Sharma C, Yusufzai MZK (2021) Friction stir channeling in AA6082 and AA2024 dissimilar alloys. Mater Today Proc 46:9469–9473. https://doi.org/10.1016/j.matpr.2020.03.237

20. Vidal C, Infante V, Vilaça P (2013) Effect of microstructure on the fatigue behavior of a friction stirred channel aluminium alloy. Procedia Eng 66:264–273. https://doi.org/10.1016/j.proeng.2013.12.081

21. Vidal C, Infante V, Vilaça P (2015) Characterisation of fatigue fracture surfaces of friction stir channelling specimens tested at different temperatures. Eng Fail Anal 56:204–215. https://doi.org/10.1016/j.engfailanal.2015.02.009

22. Pandya S, Mishra RS, Arora A (2019) Channel formation during friction stir channeling process — a material flow study using X-ray micro-computed tomography and optical microscopy. J Manuf Process 41:48–55. https://doi.org/10.1016/j.jmapro.2019.03.021

23. Kumar R, Singh K, Pandey S (2012) Process forces and heat input as function of process parameters in AA5083 friction stir welds. Trans Nonferrous Metals Soc China 22:288–298. https://doi.org/10.1016/S1003-6326(11)61173-4

24. Balasubramanian N, Mishra RS, Krishnamurthy K (2011) Process forces during friction stir channeling in an aluminum alloy. J Mater Process Technol 211:305–311. https://doi.org/10.1016/j.jmatprotec.2010.10.005

25. Vidal C, Infante V, Vilaça P (2020) Monitoring of the mechanical load and thermal history during friction stir channelling under constant position and constant force control modes. J Manuf Process 49:323–334. https://doi.org/10.1016/j.jmapro.2019.11.016

26. Karvinen H, Nordal D, Galkin T, Vilaça P (2018) Application of hybrid friction stir channeling technique to improve the cooling

efficiency of electronic components. Weld World 62:497–509. https://doi.org/10.1007/s40194-018-0576-8

27. Karvinen H, Hasani Aleni A, Salminen P, Minav T, Vilaça P (2019) Thermal efficiency and material properties of friction stir channelling applied to aluminium alloy AA5083. Energies 12:1549. https://doi.org/10.3390/en12081549

28. Vidal, C. and Vilaça P. Modular adjustable tool and correspondent process for opening continuous internal channels in solid components. 105628 T, 2011.

29. Kulekci MK, Esme U, Buldum B (2016) Critical analysis of friction stir-based manufacturing processes. Int J Adv Manuf Technol 85:1687–1712. https://doi.org/10.1007/s00170-015-8071-5

30. Pandya S, Arora A (2023) Material flow and channel geometry evolution during friction stir channeling process – Impact of tool geometry and process parameters. J Manuf Process 93:193–207. https://doi.org/10.1016/j.jmapro.2023.02.066

31. Patel NP, Parlikar P, Singh Dhari R, Mehta K, Pandya M (2019) Numerical modelling on cooling assisted friction stir welding of dissimilar Al-Cu joint. J Manuf Process 47:98–109. https://doi.org/10.1016/j.jmapro.2019.09.020

32. Vidal C, Infante V, Lage Y, Vilaça P (2013) Modelling microstructural effects on the mechanical behaviour of a friction stirred channel aluminium alloy. Key Eng Mater 577–578:37–40. https://doi.org/10.4028/www.scientific.net/KEM.577-578.37

33. Ferreira PM, Machado MA, Carvalho MS, Vidal C (2023) Granting sensorial properties to metal parts through friction stir processing. Measurement 207:112405. https://doi.org/10.1016/j.measurement.2022.112405

34. Ferreira PM, Machado MA, Carvalho MS, Vidal C (2023) Self-sensing metallic material based on piezoelectric particles. Res Rev J Nondestruct Test 1. https://doi.org/10.58286/28107

35. Fall A, Jahazi M, Khdabandeh AR, Fesharaki MH (2017) Effect of process parameters on microstructure and mechanical properties of friction stir-welded Ti–6Al–4V joints. Int J Adv Manuf Technol 91:2919–2931. https://doi.org/10.1007/s00170-016-9527-y

36. Vidal C, Alves P, Alves MM, Carmezim MJ, Fernandes MH, Grenho L et al (2022) Fabrication of a biodegradable and cytocompatible magnesium/nanohydroxyapatite/fluorapatite composite by upward friction stir processing for biomedical applications. J Mech Behav Biomed Mater 129:105137. https://doi.org/10.1016/j.jmbbm.2022.105137

37. Vidal C, Ferreira PM, Inácio PL, Ferreira FB, Santiago D, Meneses P et al (2023) Particles' distribution enhancing in aluminum-based composites produced by upward friction stir processing. Int J Adv Manuf Technol 127:2745–2757. https://doi.org/10.1007/s00170-023-11664-y

38. Moreira F, Ferreira PM, Silva RJC, Santos TG, Vidal C (2023) Aluminium-based dissimilar alloys surface composites reinforced with functional microparticles produced by upward friction stir processing. Coatings 13:962. https://doi.org/10.3390/coatings13050962

39. Sorger GL, Oliveira JP, Inácio PL, Enzinger N, Vilaça P, Miranda RM et al (2019) Non-destructive microstructural analysis by electrical conductivity: comparison with hardness measurements in different materials. J Mater Sci Technol 35:360–368. https://doi.org/10.1016/j.jmst.2018.09.047

40. Santos TG, Miranda RM, Vilaça P, Teixeira JP, dos Santos J (2011) Microstructural mapping of friction stir welded AA 7075-T6 and AlMgSc alloys using electrical conductivity. Sci Technol Weld Join 16:630–635. https://doi.org/10.1179/1362171811Y.0000000052

41. Torzewski J, Grzelak K, Wachowski M, Kosturek R (2020) Microstructure and low cycle fatigue properties of AA5083 H111 friction stir welded joint. Materials 13:2381. https://doi.org/10.3390/ma13102381